

DTIC FILE COPY

AD-A189 389

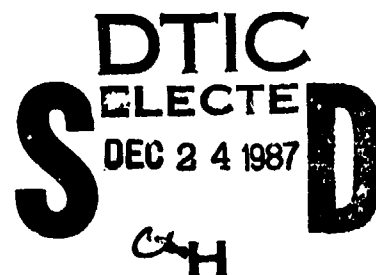


AFWAL TR-86-4070

AN INSTRUMENT FOR ADVANCED MATERIAL MICROSTRUCTURE ANALYSIS

**J. A. SMITH
R. A. HAMSTRA
J. J. LEPAGE**

**ADVANCED RESEARCH AND APPLICATIONS CORPORATION
1223 EAST ARQUES AVENUE
SUNNYVALE, CALIFORNIA 94086**



JUNE 1986

FINAL REPORT: 27 JUNE 1985 - 30 MAY 1986

APPROVED FOR PUBLIC RELEASE; DISTRIBUTION UNLIMITED

**MATERIALS LABORATORY
AIR FORCE WRIGHT AERONAUTICAL LABORATORIES
AIR FORCE SYSTEM COMMAND
WRIGHT-PATTERSON AIR FORCE BASE, OHIO 45433-6533**


87 12 11 109

NOTICE

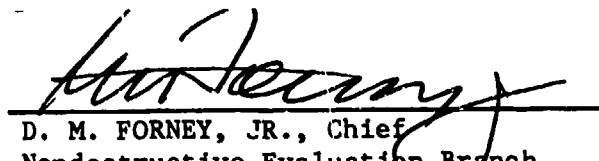
When Government drawings, specifications, or other data are used for any purpose other than in connection with a definitely Government-related procurement, the United States Government incurs no responsibility or any obligation whatsoever. The fact that the Government may have formulated or in any way supplied the said drawings, specifications, or other data, is not to be regarded by implication, or otherwise in any manner construed, as licensing the holder, or any other person or corporation; or as conveying any rights or permission to manufacture, use, or sell any patented invention that may in any way be related thereto.

This report has been reviewed by the Office of Public Affairs (ASD/PA) and is releasable to the National Technical Information Service (NTIS). At NTIS, it will be available to the general public, including foreign nations.

This technical report has been reviewed and is approved for publication.


JOSEPH A. MOYZIS, JR.
Technical Area Manager
Nondestructive Evaluation Branch

FOR THE COMMANDER


D. M. FORNEY, JR., Chief
Nondestructive Evaluation Branch
Metals and Ceramics Division

If your address has changed, if you wish to be removed from our mailing list, or if the addressee is no longer employed by your organization please notify AFWAL/MLLP, Wright-Patterson AFB, OH 45433-6533 to help us maintain a current mailing list.

Copies of this report should not be returned unless return is required by security considerations, contractual obligations, or notice on a specific document.

UNCLASSIFIED

SECURITY CLASSIFICATION OF THIS PAGE

REPORT DOCUMENTATION PAGE

1a. REPORT SECURITY CLASSIFICATION Unclassified			1b. RESTRICTIVE MARKINGS			
2a. SECURITY CLASSIFICATION AUTHORITY			3. DISTRIBUTION/AVAILABILITY OF REPORT Approved for public release; distribution unlimited.			
2b. DECLASSIFICATION/DOWNGRADING SCHEDULE						
4. PERFORMING ORGANIZATION REPORT NUMBER(S) FR-86-441			5. MONITORING ORGANIZATION REPORT NUMBER(S) AFWAL TR-86-4070			
6a. NAME OF PERFORMING ORGANIZATION Advanced Research and Applications Corporation		6b. OFFICE SYMBOL (If applicable) ARACOR		7a. NAME OF MONITORING ORGANIZATION Materials Laboratory, AFWAL/MLLP		
6c. ADDRESS (City, State and ZIP Code) Sunnyvale CA 94086		7b. ADDRESS (City, State and ZIP Code) Wright-Patterson AFB OH 45433-6533				
8a. NAME OF FUNDING/SPONSORING ORGANIZATION Materials Laboratory AFWAL		8b. OFFICE SYMBOL (If applicable) AFSC		9. PROCUREMENT INSTRUMENT IDENTIFICATION NUMBER F33615-85-C-5116		
8c. ADDRESS (City, State and ZIP Code) Wright-Patterson AFB OH 45433-6533		10. SOURCE OF FUNDING NOS.				
		PROGRAM ELEMENT NO. 6J502F		PROJECT NO. 3005		TASK NO. 50
						WORK UNIT NO. 38
11. TITLE (Include Security Classification) An Instrument for Advanced Material Microstructure Analysis						
12. PERSONAL AUTHOR(S) J. A. Smith, R. A. Hamstra, J. J. LePage						
13a. TYPE OF REPORT Final Report		13b. TIME COVERED FROM June 85 to May 86		14. DATE OF REPORT (Yr., Mo., Day) June 1986		15. PAGE COUNT 28
16. SUPPLEMENTARY NOTATION						
17. COSATI CODES			18. SUBJECT TERMS (Continue on reverse if necessary and identify by block number)			
FIELD	GROUP	SUB. GR.				
14	0	2	Nondestructive Evaluation, Computed Tomography X-ray Detectors, Tomoscope, Detector Arrays			
17	0	8				
19. ABSTRACT (Continue on reverse if necessary and identify by block number) Development and evaluation of a Scintillator Fiber-optic Reticon Detector array (SFRD) for application to a high-resolution computed tomography (CT) instrument, or Tomoscope, has been carried out. The objectives were to develop cryogenic cooling and electronic control and amplification to improve the detector noise performance and to evaluate the thermal, electronic and X-ray performance of the detector package. The thermoelectric cryostat was developed with a temperature floor of -70°C and typical drift of 0.1°C/min. The electronic control allows computer adjustment of integration time between .18 and 350 seconds. The preamplifier demonstrated RMS noise of order 1000 electrons, though the overall system noise was significantly higher. X-ray testing demonstrated detector resolution better than 50-microns FWHM. The Tomoscope will be a valuable instrument for NDE evaluations, aerospace materials and components. In particular, for inspection of internal structure and damage of materials used in turbine blades, vanes and disks. It will be useful for better understanding of fabrication, failure modes and for final component inspections.						
20. DISTRIBUTION/AVAILABILITY OF ABSTRACT UNCLASSIFIED/UNLIMITED <input type="checkbox"/> SAME AS RPT. <input checked="" type="checkbox"/> DTIC USERS <input type="checkbox"/>			21. ABSTRACT SECURITY CLASSIFICATION Unclassified			
22a. NAME OF RESPONSIBLE INDIVIDUAL MICHAEL D. POLOVINO, 1Lt, USAF			22b. TELEPHONE NUMBER (Include Area Code) (513) 255-5309		22c. OFFICE SYMBOL AFWAL/MLLP	

ACKNOWLEDGEMENTS

The authors would like to acknowledge the invaluable contributions of Edward Franco, Bart Jackson, and Brian Rodrigues in the design and implementation of the experimental apparatus and software used in this project.



Accession For	
NTIS GRA&I	<input checked="checked" type="checkbox"/>
DTIC TAB	<input type="checkbox"/>
Unannounced	<input type="checkbox"/>
Justification	
By	
Distribution/	
Availability Codes	
Dist	Avail and/or Special
A-1	

TABLE OF CONTENTS

<u>Section</u>	<u>Page</u>
ACKNOWLEDGEMENTS.	i
TABLE OF CONTENTS	ii
LIST OF FIGURES	iii
LIST OF ILLUSTRATIONS	iii
1.0 INTRODUCTION.	1
1.1 Tomoscope Program Significance	1
1.2 Report Organization.	2
1.3 High Resolution CT Concept	3
1.4 Program Goals.	7
1.5 Overview of Accomplishments.	8
2.0 DETECTOR NOISE ANALYSIS	9
3.0 CRYOSTAT DESIGN AND PERFORMANCE	15
3.1 Design Concept	15
3.2 Performance Tests.	17
3.3 Assessment	19
4.0 SIGNAL PROCESSING DESIGN AND PERFORMANCE.	19
4.1 Design Concept	19
4.2 Performance Tests.	22
4.3 Assessment	23
5.0 X-RAY TESTING	23
5.1 The Experiment	23
5.2 Assessment	27
6.0 CONCLUSIONS	28
REFERENCES.	29

LIST OF ILLUSTRATIONS

<u>Figure</u>		<u>Page</u>
1	Tomoscope Rotate-Only Scan Geometry.	4
2	Scintillator Fiber-Optic Reticon Detector (SFRD) Layout.	5
3	Design Drawing of SFRD Cryostat.	16
4	Cryostat/Detector Assembly Photographs	18
5	Block Diagram of Reticon Control and Analog Signal Processing Circuitry.	20
6	Measured Point-Spread Response of SFRD	25
7	Modelled Point-Spread Response of SFRD	26

LIST OF TABLES

<u>Table</u>		
1	Allowable integration times and thermal drift rate to maintain shot noise and thermal instability to 500 electrons RMS.	13
2	Thickness of selected materials required to attenuate 80 keV x rays by 100.	14

1.0 INTRODUCTION

This document is submitted as the Final Report of research activities conducted under Air Force contract F33615-85-C-5116, a Phase I SBIR with the objective of developing and demonstrating the capabilities of an efficient high-resolution detector array. This array, the Scintillator Fiber-Optic Reticon Detector (SFRD) has been targeted as a detection technology appropriate to the development of a high-resolution computed tomography instrument -- the Tomoscope.

1.1 Tomoscope Program Significance

A number of high-temperature materials have been developed to meet special Air Force applications. An important example of the use of these materials is in critical turbine engine components, such as blades, vanes, disks, and various other parts. Impelled by significantly more stringent performance requirements, there is a strong interest in developing improved processing techniques and/or new families of materials which will greatly extend the physical properties of such materials. For instance, high-temperature alloys are sought which possess substantially lower creep, fatigue, and oxidation rates than current materials. New ceramics with more reproducible processing characteristics and better thermal stress and fracture reliability are in demand, and oxidation-resistant advanced composites are needed for use above 3000°F.

The key to the development of these new higher-performance, lighter-weight structures is an understanding of the properties and behavior of these advanced materials as a function of their microstructure. An inspection method is needed to guide the emergence of this understanding. The ideal method would be one which is non-destructive in nature, capable of sizing and locating defects to a resolution of 25 microns or better, and able to provide quantitative information about material composition and structure. Without the availability of such a technique, the timely development of these advanced materials could be adversely affected. Thus, to a large extent, the successful creation of reliable high temperature materials is dependent on the development of an inspection technique which can conveniently and non-destructively elicit the microstructural properties of materials.

This project is a key step in a program to develop an improved NDE instrument, an x-ray tomoscope with features specifically designed to meet Air Force materials research requirements. This instrument, which is based on computed-tomography (CT) principles, is expected to have the properties attributed above to the "ideal" NDE instrument, including the ability to provide accurate, high-resolution images in three-dimensions of defects/damage in a wide range of materials.

Previous work for the Defense Nuclear Agency has established the general efficacy of such an instrument.(1) The equipment of any CT system, independent of the computer hardware and its associated peripherals, consists of three basic elements: the x-ray source, the x-ray detector, and the mechanical handling system. The earlier work demonstrated the existence of satisfactory source and detector technologies, the key areas of technical uncertainty. Performance improvements for the prototype detector designed and built specifically for this application are the impetus behind this project.

1.2 Report Organization

Section 1.3 provides an introduction to the Tomoscope concept, in particular, to the SFRD technology addressed in this report. Sections 1.4 and 1.5 summarize the project objectives and accomplishments. Section 2 gives a detailed analysis of the cause, cure and implications of the various noise contributors impacting SFRD performance.

In Sections 3 and 4 we discuss the design, implementation and performance of the detector cryostat and interface electronics which constituted the heart of the project effort. Section 5 presents the x-ray experiments which evaluated the spatial resolution performance of the SFRD, and Section 6 summarizes the overall project accomplishments and the reassessed outlook with regard to the development of the Tomoscope.

1.3 High Resolution CT Concept

A common driver in diagnostic measurements is the quest for more information with improved quality and detail -- e.g. better resolution in space, time, spectrum etc. -- until the available techniques are pushed to their limit. The current efforts to develop higher spatial resolution CT instrumentation is no exception to this rule. In this case, the parameter which is most severely stressed is the instrumental throughput. In particular, the requirement for detailed spatial resolution in practical measurements runs into the requirement for a sufficient number of transmitted photons to provide the information required for image reconstruction. Available fluxes are limited by present-day x-ray source technology.

In this context it is clear that a practical approach to high resolution CT necessitates optimization of the scan geometry and detector efficiency to make use of as much of the available signal strength as possible. Our approach to this problem is embodied in the Tomoscope concept illustrated in Figure 1. The concept uses a "rotate-only" geometry which maintains the scan object entirely in the x-ray fan, and a paved detector surface to intercept all of the available x rays. The implementation of a low-noise detector with a high quantum detection efficiency such that signal resolution is limited by the statistical variations inherent in the finite signal intensity effects an optimum design, leaving the onus for further throughput improvements on the development of advanced high-intensity sources.

The detector, which we have designated the SFRD for Scintillator-Fiber optic-Reticon Detector, is illustrated in Figure 2. The Reticon is an array of individual silicon photodiodes, each with an associated storage capacitance on which to integrate photocurrent, and a multiplex switch for periodic readout via an integrated shift register scanning circuit. The S-series array, used in these experiments, consists of 1024 of these sensor elements located on 25 micron centers for a total length of 25.6 mm. Each element is, in addition, 2.5 mm in length. The Reticon photodiodes are initially charged to 5 V before exposure. Light incident on the sensors produces electron-hole pairs in the silicon which drain off this charge. The total exposure is determined by measuring the charge required to recharge the diode capacitance.

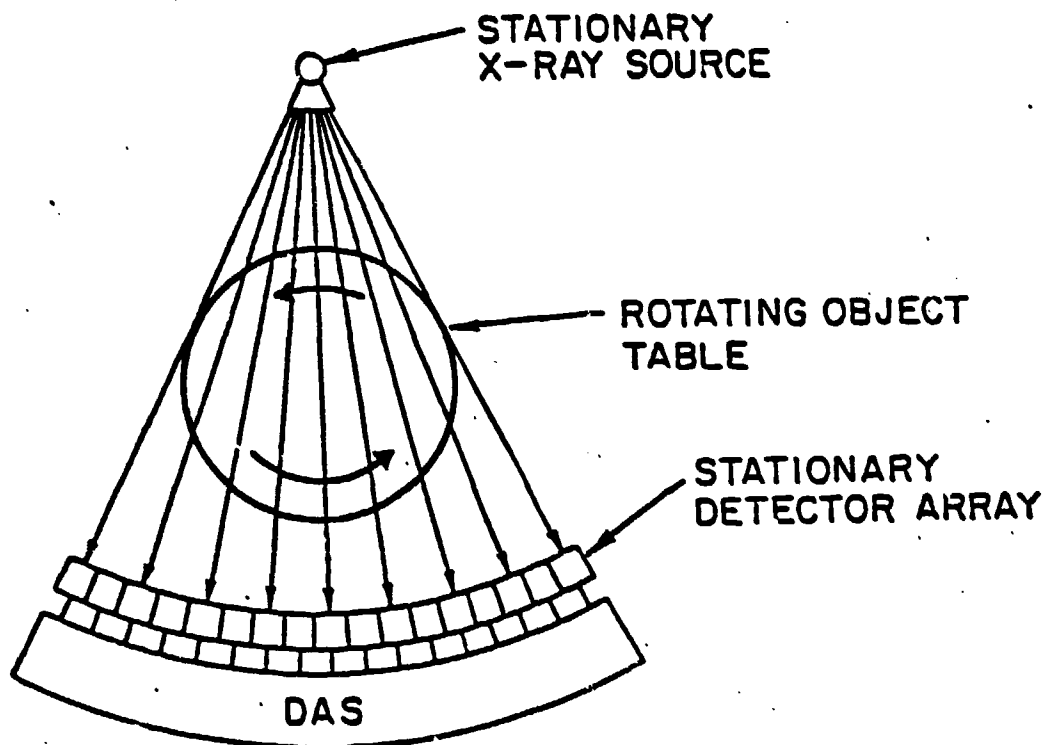


Figure 1. Tomoscope Rotate-Only Scan Geometry

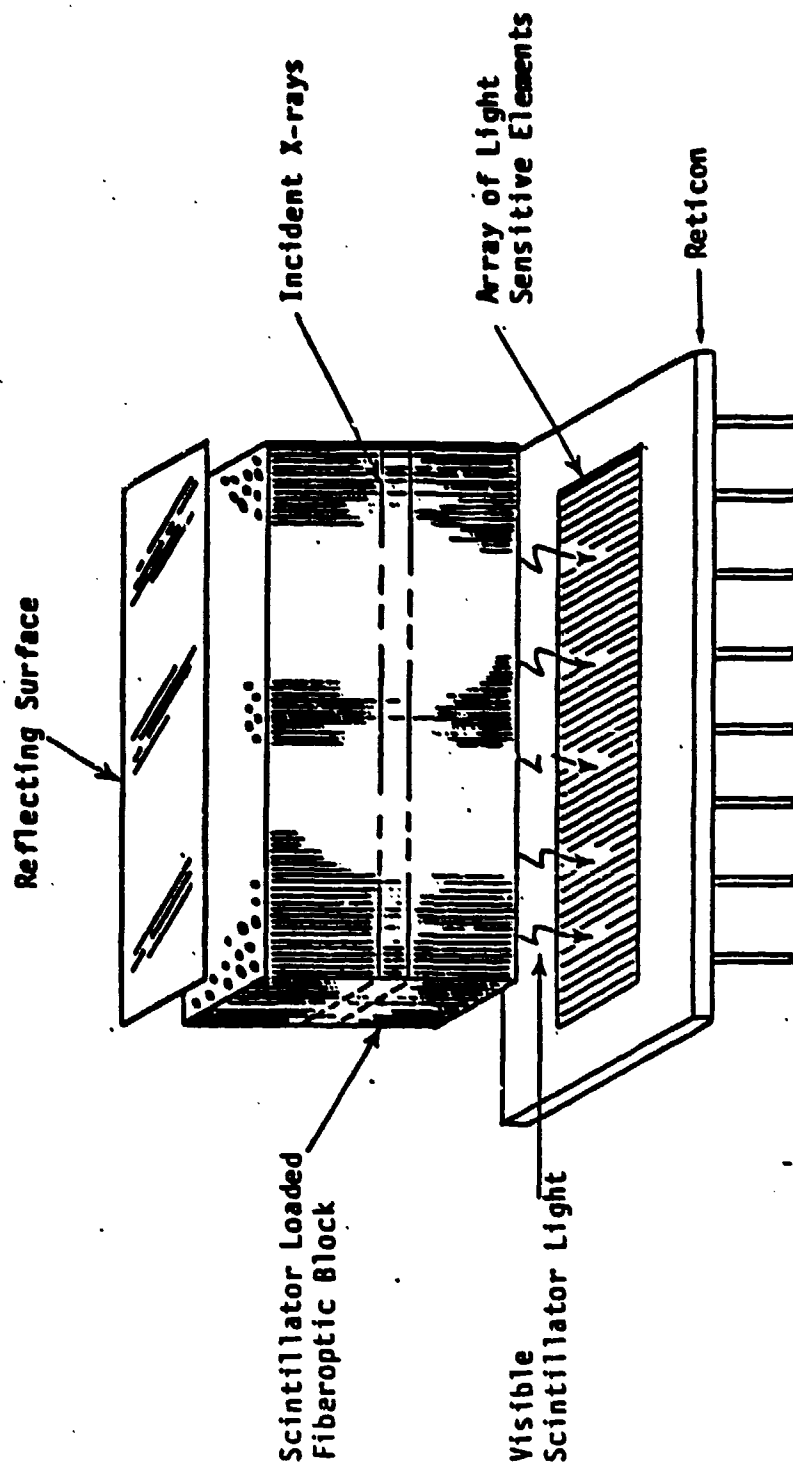


Figure 2. Scintillator Fiber-Optic Reticon Detector (SFIRD) Layout

The scintillator chosen for initial evaluation of the technology was provided by Synergistic Detector Designs (Mountain View, CA.). The properties appear compatible with the ultimate goals of high quantum efficiency for incident x rays and inherent resolution of order 25 microns. The scintillator consists of a fiber-optic block with the individual fibers loaded with a barium based scintillator and clad with EMA (Extra-Mural Absorber) that reduces optical crosstalk between fibers. The fibers are spaced on 25-micron centers and are interfaced to the Reticon through a fiber-optic facplate which is not shown in Figure 2. The scintillator thickness of 2.5 mm is designed to match the photodiodes. The inclusion of barium in the fibers tailors the absorption characteristics to the prospective tungsten x-ray spectrum.

The x rays absorbed in the scintillator excite photoelectrons which cause scintillation in the visible portion of the spectrum. This light is conducted by the fibers to the Reticon photodiodes where it is detected. We have estimated that approximately ten scintillation photons are absorbed in the sensors for each x ray absorbed in the fibers. As long as this number is significantly greater than one, the effect of scintillator shot noise (associated with variations in detected current per x ray) will be negligible.

Initial experiments at TFI Corporation in Connecticut showed that the Reticon would require cooling to reduce dark current thermal drift and shot noise. In addition the Reticon control board which was procured with the detector package was a general purpose evaluations board essentially designed for video applications. To extract the performance inherent in the Reticon would require development of a design specifically tailored to the demands of x-ray measurements.

1.4 Program Goals

This project addresses detector noise reduction questions and further evaluation of detector performance. The stated goals of this project are:

- o Design and Implement a Low Temperature Detector Cryostat:

For a given integration time, a fraction of the stored charge on the photodiodes will drain off due to thermal conductivity in the silicon. This dark current is strongly temperature dependent -- for example, typical dark currents at 20°C, -40°C and -70°C are 10^{-11} A, 10^{-14} A and 5×10^{-16} A, respectively. At room temperature, it takes about 5 seconds to completely discharge a photodiode. Even more problematical than the obvious reduction in integration time are the shot noise associated with the dark current and the sensitivity to thermal drift.

The first objective of this program was to design and construct a detector cryostat to cool the detector package to -40°C in order to limit the dark current shot noise and to stabilize the temperature.

- o Design and Build Low Noise Control and Signal Processing Electronics:

As discussed earlier, the original control electronics for the Reticon were designed for video output. In particular, the signal amplification was too noisy, the output performed a DC restoration on the signal which was not sufficiently stable, integration time adjustments were via on-board switches and operated by varying the clock rate (which is inappropriate for precision ADC conversion), and the circuitry involved numerous video related adjustments which are not useful for the present application and probably further degrade performance.

The second objective of the program was to redesign and implement the control and detection circuitry to provide precision low-noise signal detection and stable circuit control customized for the anticipated usage parameters.

o Evaluate Detector Package Performance:

The previous experiments at TFI served to delineate the problems associated with thermal and electronic noise but were not able to substantially address the x-ray performance of the detector package.

The third objective of this program was to evaluate the performance of the detector package. This includes the thermal characteristics of the cryostat, the stability and noise floor of the electronics and the x-ray resolution characteristics of the detector. In addition, the performance was to be evaluated on a ceramic phantom test object.

1.5 Overview of Accomplishments

This project undertook an ambitious technology development effort at which it was largely successful. At initiation, the specific task objectives were analyzed. The objectives were more specifically determined, particularly with respect to the thermal and electronic performance. The basic design philosophy was to pursue these objectives to levels approaching the fundamental limits of the technology. The rationale for this approach was to understand the problems involved in achieving what we see as the capabilities of this technology, and to avoid the necessity of having to readdress these same issues as we approach the demanding requirements of an efficient high-resolution CT inspection system. Below we have abstracted the accomplishments of this program. All of the stated goals of the project have been accomplished except for the ceramic test-piece which was not done because of funding limitations.

o Detector Cryostat Designed and Constructed:

Performance was Demonstrated to -50°C .

Projected Temperature Limit -70°C .

Thermal Stability Better than $0.1^{\circ}\text{C}/\text{min}$.

Dark Current Suppressed by 10^3 .

o Electronic Control and Analog Signal Processing Designed and Constructed:

Amplifier Bench Tested to 1000 electrons RMS noise.

Facility Implementation demonstrated $\text{S/N } 3 \times 10^3$.

Integration times computer controlled from 175 ms to 350 s.

Circuit stability excellent.

o X-ray Performance Characterization:

Point-Spread-Function has <50 micron FWHM with a broad underlying tail

Pseudoscan of ceramic piece was not done.

2.0 DETECTOR NOISE ANALYSIS

We can summarize the technical goals of this project as reduction of the Reticon noise contributions through cooling and electronic redesign and evaluation of the resulting detector package. An important first step in this process was to set design goals for the noise reduction efforts. Determining these goals, in essence, consists of setting a noise budget, evaluating the range of integration periods through which the detector must remain within the noise budget, and determining the allowable contributions to this budget from the individual noise sources.

Setting the noise floor is equivalent to determining the dynamic range of the instrument. In this report we will use the term dynamic range to refer to the ratio of the maximum unattenuated x-ray signal to the minimum x-ray signal which can be measured efficiently (limited only by photon statistics). This is distinct from the signal to noise ratio (S/N). In practice, the maximum

unattenuated signal, N_{\max} , is determined from the saturation charge of the Reticon, Q_{sat} , and the scintillator conversion charge, Q_{scn} .

$$N_{\max} = Q_{\text{sat}}/Q_{\text{scn}} \quad \text{Eqn. 1}$$

Q_{sat} (9×10^7 elec.) is set by the photodiode capacitance (14 pF) and the charging voltage (5 V). Q_{scn} is determined by the conversion efficiency of the scintillator, the acceptance angle of the optical fibers, the transmission through the fibers and fiber-optic plate, reflections at the interfaces, and the light conversion efficiency of the photodiodes. We have estimated that Q_{scn} is about ten, and will use $N_{\max} = 10^7$ x rays (per photodiode). This Figure is good to about a factor of two -- subject to experimental determination.

As long as the uncertainty in the most attenuated signals is dominated by photon statistics (shot noise), the noise in the final image can be efficiently reduced by either longer exposures or repeated measurements of the same view. This type of noise dependence is explicitly assumed in formulas for contrast discrimination and contrast sensitivity. If the attenuation of x rays through a portion of a test object is high enough that the uncertainty is dominated by noise in the detection system then the local image noise will be correspondingly higher. Further image improvements would require multiple samples to average over the detector noise and would become increasingly inefficient. Note, however, that the system will be able to image detail to considerably higher attenuations than the defined dynamic range. As long as the contrast is high enough that the increase in noise is not prohibitive, the ultimate floor is set by the ability to see features above the detector noise.

The dynamic range, R_d , can be expressed in terms of the total electronic noise, Q_{tot} , by setting the photon shot noise of the minimum "efficiently" measurable signal (N_{\min}) equal to the electronic noise.

$$\begin{aligned} (N_{\min})^{1/2} * Q_{\text{scn}} &= Q_{\text{tot}} \\ R_d = N_{\max}/N_{\min} &= (Q_{\text{sat}} * Q_{\text{scn}})/Q_{\text{tot}}^2 \end{aligned} \quad \text{Eqn. 2}$$

The noise sources which contribute to Q_{tot} are the pixel reset noise, Q_p , dark current shot noise, Q_{shot} , dark current thermal drift, Q_{drift} , preamplifier noise, Q_{pre} , post-preamplifier circuit noise, Q_{post} , and digitization noise, Q_{dig} . The one component which is beyond our control is the pixel reset noise -- due to thermal variations in the charge stored in the pixel capacitance. For the Reticon 1024S used in these experiments this variation is about 1000 electrons decreasing only slightly at reduced temperatures. This 1000 electron limit sets a practical target for the other contributions to the electronic noise. Essentially, if the other components can be reduced to half of this number their contribution to the overall noise budget is minimal and further efforts would be wasteful. Note that the separate noise components add in quadrature. On the other hand, any component which is greater than 1000 electrons quickly becomes the dominant noise source and warrants extra effort toward its reduction.

At the beginning of this project we were aware that previous low-noise implementations of Reticon circuitry had achieved preamplifier noise characteristics of about 1000 electrons.⁽²⁾ This "existence theorem" and the considerations discussed above led us to select a design target of 1000 electrons for the preamplifier circuitry.

The dark current shot noise is caused by statistical variations in the current drained out of the individual photodiodes which is a strong function of temperature. Below room temperature, typical values for this current, taken from the manufacturers specifications are:

$$I_{dark} = I_0 \exp(T/T_0) \quad \text{Eqn. 3}$$

$$I_0 = 3 \times 10^{-26} \text{ A} ; T_0 = 8.7 \text{ K}$$

The temperature is expressed in kelvins. The time integrated charge, Q_d , and corresponding shot noise can be expressed in terms of the integration period.

$$Q_d = I_{dark} * t_{int} = N_d * q_e \quad \text{Eqn. 4}$$

$$Q_{shot} = (N_d)^{1/2} * q_e$$

$$= 1/q_e (I_0 \exp(T/T_0) * t_{int})^{1/2}$$

N_d is defined as the number of electrons (electron charge = q_e) in the time integrated dark current.

Thermal variations in this charge are simply due to the change in temperature between dark current measurements and the corresponding x-ray measurements. In a practical instrument it would be desirable to reduce the frequency of dark current measurements to a fraction of the x-ray exposures to limit the impact on the overall throughput. The maximum allowable thermal drift would correspond to a single integration period. The noise, Q_{drift} , associated with this thermal drift (temperature change = T_d , can be expressed by substituting Eqn. 3 in Eqn. 4, taking the derivative and simplifying the result:

$$Q_{drift} = T_d/T_0 * Q_d \quad \text{Eqn. 5}$$

The Reticon used in the present experiments is specified by the manufacturer to -40°C . This limit is set by the fiber-optic faceplate which is bonded to the face of the Reticon. Differential thermal contractions can damage the Reticon at lower temperatures. If the package is redesigned to remove this bonded interface, the Reticon is specified to -70°C . To enable future experiments to be performed at the lower temperature, the present cryostat design target was set at -70°C as the added expense of maintaining this flexibility was not great.

To put equations 3 to 5 in perspective, we have summarized in Table 1 the maximum integration time and temperature changes which can be allowed while keeping the dark current shot noise and thermal drift at the 500 electron level for temperatures of 20, -40 and -70°C .

Table 1: Allowable integration times and thermal drift rate to maintain shot noise and thermal instability to 500 electrons RMS.

	20°C	-40°C	-70°C
Integration Period: (seconds)	.003	3	100
Temperature Change: (K per minute)	350	.35	.01

Note, that if the noise budget is loosened to 1000 electrons for each of these components, the allowable integration time is quadrupled (Eqn. 4) and the allowable drift rate is halved (Eqn. 4 and 5). In the present project, no attempt was made to feedback regulate the temperature as the requirements listed above are not particularly stringent, the insulation inherent in the cryostat would substantially stabilize the temperature and it was considered prudent to observe the thermal stability and response times of the design before determining the requirements for more elaborate control.

Post-preamplifier noise includes any noise which is picked up between the preamplifier stage and the digitizer. In general, this can always be reduced to levels below the preamplifier noise, however, in practice, this is a task which requires particular care in circuit layout and detailed troubleshooting of the final design. Charge sensitive circuitry, such as that used in the present effort, is particularly sensitive to noise pickup.

The RMS quantization noise associated with perfect digitization of an analog signal is generally expressed in terms of the single bit conversion ratio, Qbit:

$$Q_{dig} = Q_{bit}/(12)^{1/2} \quad \text{Eqn. 6}$$

To achieve less than 500 electrons noise this would require a 6-bit digitizer. In lieu of perfect digitizers, an eventual design using at least 18 bits would be advisable. In the present project we used an available 13 bit digitizer for reasons of economy and because this was not a design parameter under investigation.

If we now assume the eventual noise goals of 1000 electrons for Q_p and Q_{pre} and 500 electrons for Q_{shot} , Q_{drift} , Q_{post} and Q_{dig} we find:

$$Q_{tot} = (\sum Q_i^2)^{1/2} = 1730 \text{ electrons.}$$

If we substitute this value in Eqn. 2, we obtain a dynamic range of 300:1. Even allowing for some shortfall in these eventual noise goals and the factor of two uncertainty in Q_{scn} , a dynamic range of 100:1 appears reasonable (see Eqn. 2). To put this conclusion in perspective, we have listed in Table 2 the thickness of several materials which would attenuate 80-keV x rays (the approximate mean energy of a 200 kV Tungsten spectrum) by a factor of 100. In practice, hardening of the spectrum would increase the penetration somewhat.

Table 2: Thickness of selected materials required to attenuate 80 keV x rays by 100.

Material	Assumed Density (g/cm ³)	Thickness (cm)
Carbon	2.0	14.3
SiO ₂	2.3	10.3
Bone	1.85	11.9
Aluminum	2.7	8.4
Iron	7.86	.98
Copper	8.96	.67
Tungsten	19.3	.03
lead	11.3	.17

As shown in the table, a dynamic range of 100:1 would be able to efficiently image substantial amounts of low atomic number materials and in particular the composites addressed in this project. In addition small objects or inclusions of ferrous metals would be manageable. High-Z materials could of course only be tolerated in small amounts.

3.0 CRYOSTAT DESIGN AND PERFORMANCE

Based on the considerations discussed in section 2.2, the cryostat design strategy was to provide the capability of cooling to -70°C for ultimate flexibility, though the present tests would only go down to -40°C due to the temperature limits of the present Reticon. In addition, while the prototype would not be feedback regulated, it should be designed to be thermally stable and should provide for straightforward and flexible addition of regulation as required.

3.1 Design Concept

The cryostat is illustrated in the design drawing of Figure 3. The assembly, viewed here from the side, consists of a pyramid of three thermoelectrically cooled stages and a high capacity water-cooled copper heat-sink. The detector assembly (including preamplifier) mounts on the upper stage.

The cooling is accomplished by means of commercially available thermoelectric modules. These modules are thin sandwiches containing an array of cooling elements known as couples. Each couple consists of a pair of bismuth alloy semiconductors (one n-type, one p-type) connected electrically in series and thermally in parallel (that is side by side). When an electric current is passed through the couple, heat is transferred across the couple via the Peltier effect. Because of I^2R heating in the couples, each stage dumps substantially more heat into the following stage than it removes. Thus, in a multistage design, the lower stages must carry more heat and consequently utilize more couples than the preceding stages. In the present design, the first stage uses one module containing thirty-one couples, the second stage four modules (thirty-one couples per module) and the third stage nine modules (forty-nine couples per module). The package was designed to handle up to two watts of power load at -70°C . As the load turned out to be approximately one watt, this left a comfortable margin in the design.

The cryostat is designed as a series of three nested boxes, or stages, with the entire assembly mounted inside a vacuum enclosure to eliminate atmospheric

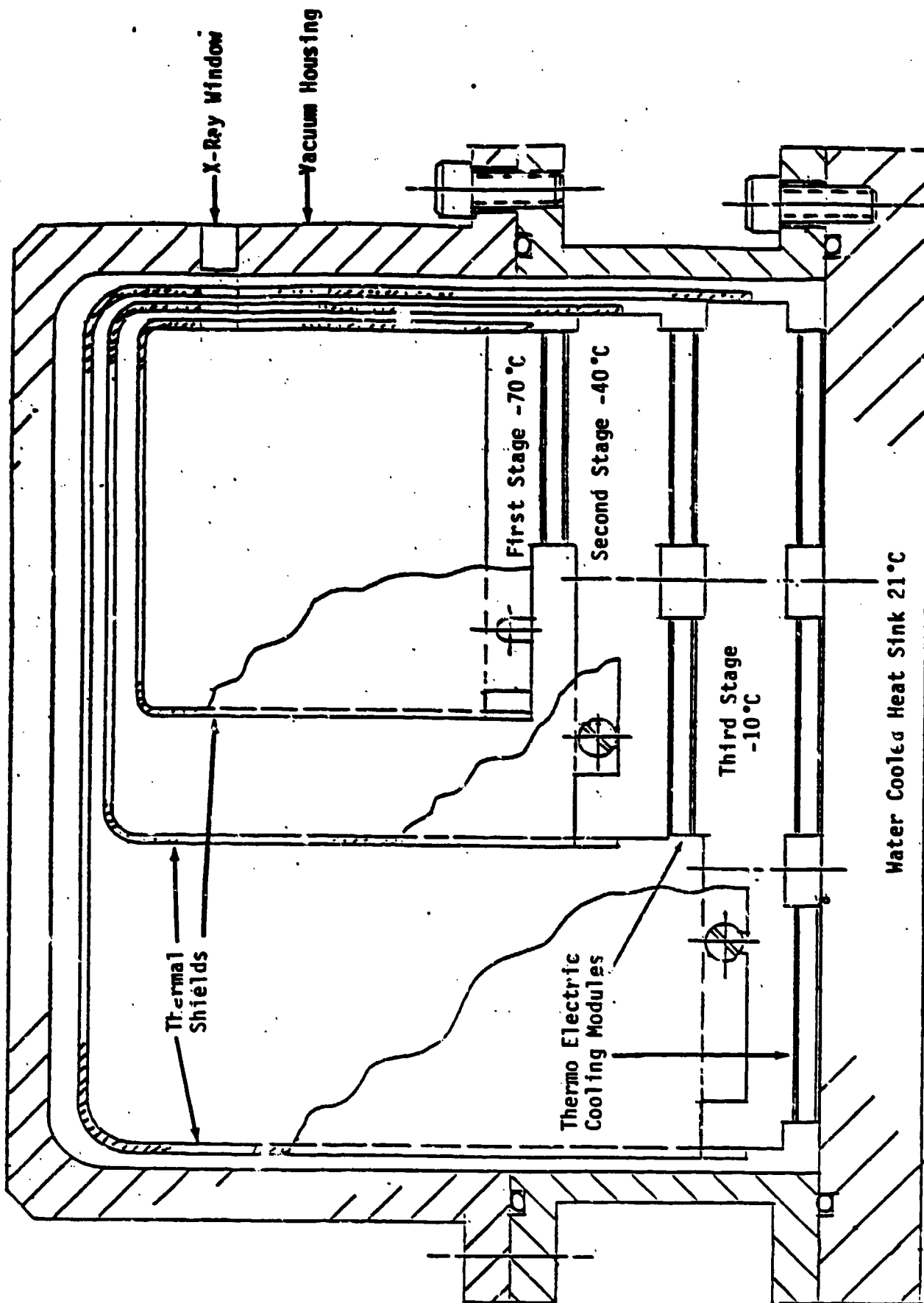


Figure 3. Design Drawing of SFRD Cryostat

heat transfer and condensation. Each stage includes a cover made from a drawn aluminum can to reduce transmission of thermal radiation from higher temperature to lower temperature stages. Each cover is mounted on an aluminum heat sink and has a cutout window, covered by aluminum foil, to limit x-ray absorption and scatter, while providing thermal and electrical isolation. X-ray access was provided through a .02-inch-thick window milled into the aluminum vacuum cover.

The temperature of each stage is monitored by a PTAT (Proportional To Absolute Temperature), which as the name implies, acts as a stable current source whose output is proportional to absolute temperature.

The selected design has several noteworthy features. Use of multiple isolated stages provides excellent thermal insulation and because of the comparatively long stage-to-stage response time (about 15 minutes), substantial attenuation of external thermal transients. In addition, each stage can be separately grounded -- contributing to noise reduction. The use of electrical temperature control and monitoring lends itself to simple and flexible feedback regulation if necessary.

The entire vacuum package is shown at selected stages of construction in Figure 4. Included are (a) the electronic stage and Reticon before and (b) after mounting the scintillator block; (c) after the third cover has been mounted; and (d) after the outer vacuum cover has been mounted.

3.2 Performance Tests

The detector package was evacuated to a few millitorr. The thermoelectric modules were turned on and the system brought down to operating temperature in about 30 minutes. The first time this was done, the temperature was inadvertently dropped to -50°C due to an improperly selected sensing resistor. On subsequent experiments the temperature was maintained at -40°C . It was clear, however, from the systems thermal response and from the need to operate the modules at well below their maximum capacity that the design goal of -70°C could be attained. Due to the complex relationship between module current, efficiency and temperature it is difficult to simply demonstrate this, however

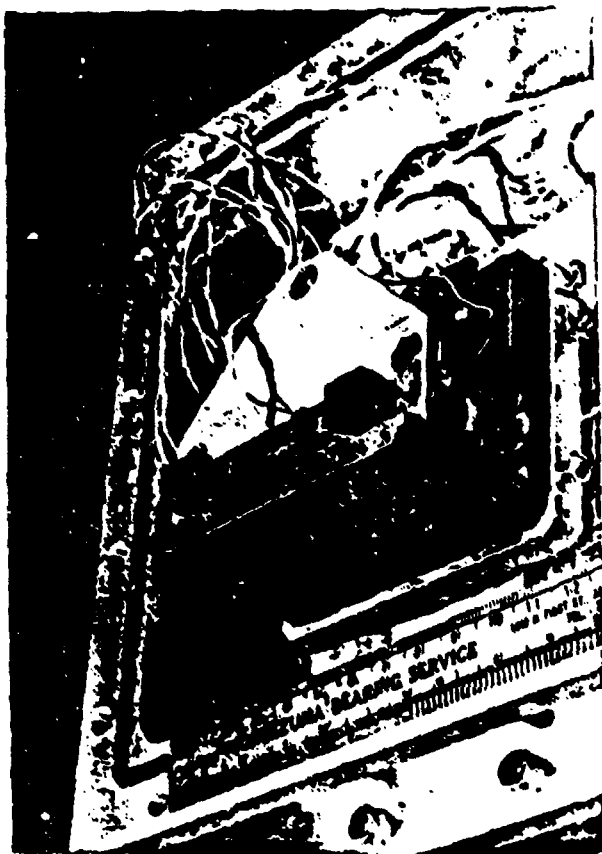


Figure 4.A. Reticon and Electronics Mounting



Figure 4.B. Scintillator-Fiber-Optic Mounted

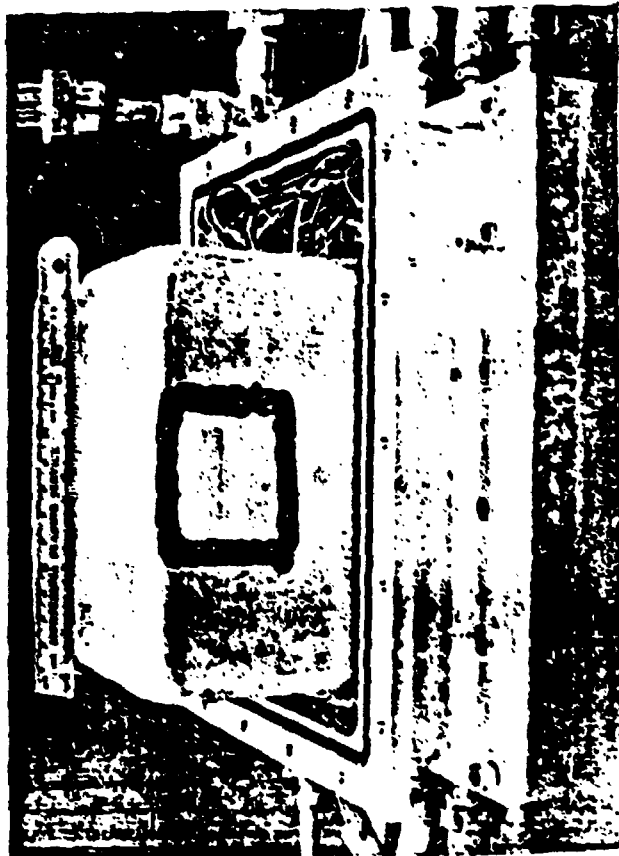


Figure 4.C. Outer Thermal Shield Installed



Figure 4.D. Vacuum Housing with X-Ray Window

the performance was consistent with the design model assuming a first stage power load of 1 watt as opposed to the 2 watt design capacity.

Thermal drift was normally about $.005^{\circ}\text{C}$ per minute. At most the drift reached 0.1°C per minute about 20 minutes after the facility air conditioning was turned off at which time the ambient temperature had increased by several degrees. Referring to Table 1, we can see that the cryostat is sufficiently stable for all but the longest integration times without further temperature regulation.

3.3 Assessment

The cryostat design was completely successful. It is clear that the design temperature of -70°C is possible. The low thermal drift indicates that little or no regulation (other than use of regulated current supplies for the modules) would be necessary unless the most stringent requirements of 100 second integration times are used.

4.0 SIGNAL PROCESSING DESIGN AND PERFORMANCE

The electronic design objectives were to design and implement: (1) an analog preamplification and processing circuit capable of detecting the signal levels with 1000 electrons RMS noise; and (2) a control board capable of stably operating the Reticon under computer selected integration times from 200ms to 100 sec.

4.1 Design Concept

A block diagram of the Reticon control and amplification circuitry is shown in Figure 5. Of particular interest is the signal amplification strategy. The output of the Reticon consists of sequentially switching the individual photodiodes onto the two video lines in an alternating pattern. By measuring the charge required to restore these pixels, the circuit determines the integrated exposure over the preceding time period.

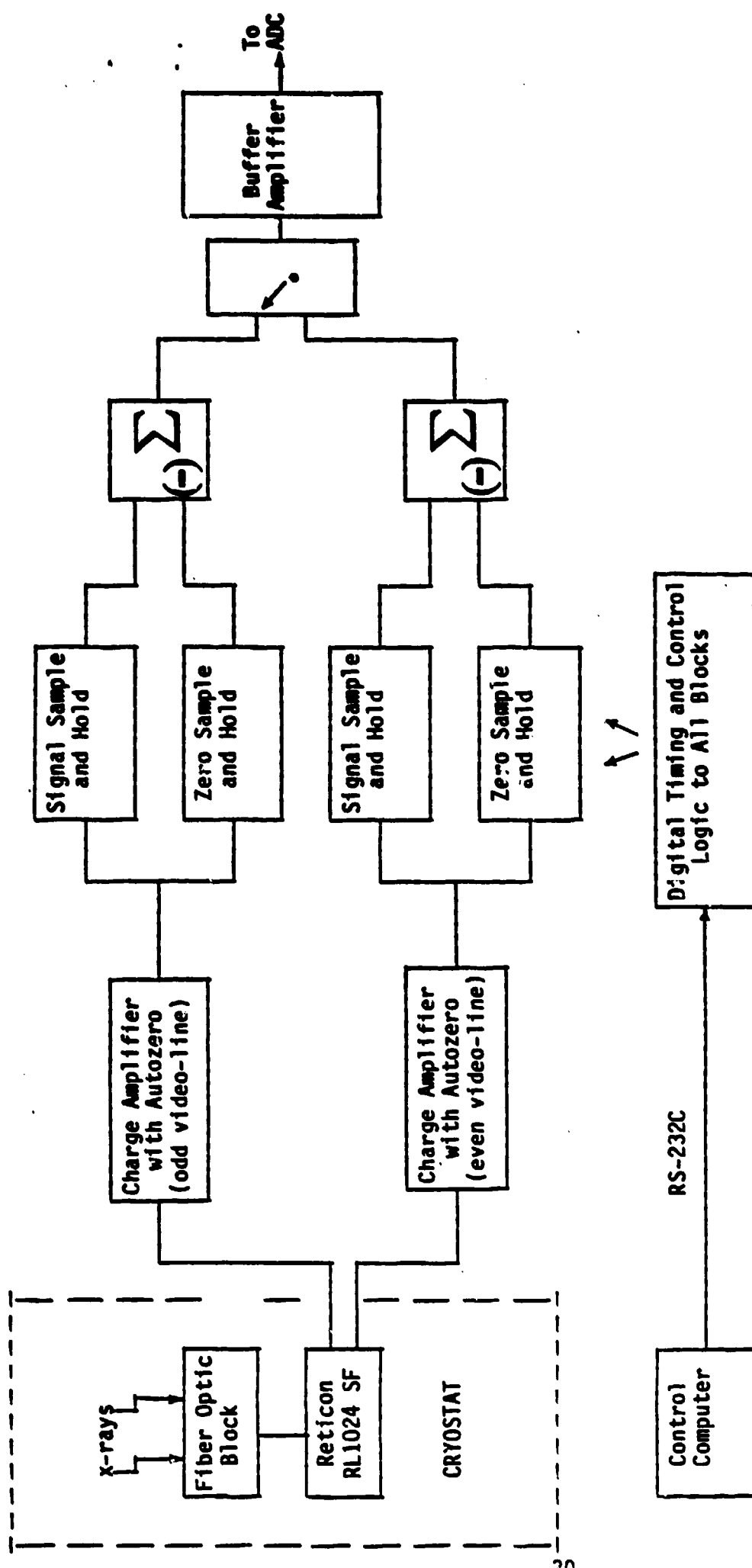


Figure 5. Block Diagram of Reticon Control and Analog Signal Processing

Signal detection involves a sequence of steps which are repeated, alternating between the odd and even video lines until all 1024 pixels have been sampled:

- 1) Reset integrator and video line.
- 2) Sample and hold "zero" value.
- 3) Connect photodiode to video line and integrate recharge current.
- 4) Sample and hold integrated signal charge.
- 5) Subtract "zero" value from signal charge.
- 6) Switch net signal to output buffer amplifier.

This technique, known as double correlated sampling, is employed to correct for charge injected onto the video lines by the solid state switches in the reset operation. The preamplifier circuitry is located on the top stage of the cryostat along with the Reticon to limit noise pickup and input capacitance by shortening the signal path and to reduce thermally generated preamplifier noise and drift.

The buffer amplifier outputs the signal (at this point consisting of packets of 1024 pulses, with packet separations equal to the integration period) to the digitization circuitry. In this project, the digitizer is located in the data acquisition system (DAS) CAMAC bin in the control room. In the fully-developed system, this digitization would be performed on the control board to prevent noise pickup in the long signal run.

The control circuitry provides supply voltages, a four phase clock to time the shift register readout of the diodes and a start pulse to initiate the readout. Integration time is adjusted by varying the timing of the start pulse. The start pulse is generated by using a two scalar chips to divide down the clock pulse. An RS-232-C signal input from a terminal or from the scan control computer controls selection of the appropriate time interval by multiples of two.

The implemented integration range, 175 millisecond to 350 seconds was selected to encompass the range of values we considered plausible for the current and prospective uses. The lower limit is set by the frequency bandwidth

of the preamplifiers and could be shortened by another factor of two. The upper limit could be extended indefinitely, if the need arose.

4.2 Performance Tests

Performance testing consisted of bench tests of the circuitry and installation tests of the components installed in the cryostat and connected to the CAMAC DAS in the control room.

The preamplifier/sampling circuitry was bench tested by leaving the video line inputs open and displaying the repetitive output waveform on a sensitive oscilloscope. The width of the overlayed output traces was 0.1 mV (full output is 8 V) corresponding to a noise level of approximately 1000 electrons as desired. The control circuitry performed as designed providing a stable pattern for all integration periods.

After installation in the cryostat, the circuitry was connected to the DAS and cooled to -40°C . In this configuration, the noise level was evaluated by statistically analyzing the scan as digitized by the available 8 V, 13-bit digitizer. The measured pixel standard deviation was 3 counts which corresponds to 3 mV or about a 30 times increase in the noise level. The source of the extra noise pickup is not known but could lie in the layout and grounding details within the cryostat and/or in the fifteen foot signal run to the DAS. The latter is probably a significant contributor because the unbalanced input to the digitizer makes it sensitive to noise induction. We did not pursue the source of the noise pickup as this type of troubleshooting can be very time intensive and the present level was adequate to perform the x-ray characterizations. Nevertheless, the quality of the bench tests gives us confidence that noise levels approaching the 1000 electron level can be achieved by careful work. In addition, the difficulties posed by driving an unbalanced input over several feet will not be required in a final design as the digitization circuitry will be moved onto the control board.

The Reticon control circuitry worked as designed in the installed configuration. The signals were stable and properly synchronized for all selected integration periods.

4.3 Assessment

The electronic control and amplification design was largely successful. The one difficulty encountered -- a high level of post-preamplifier pickup -- does not appear to be a fundamental problem and should lend itself to a thorough troubleshooting investigation. In addition much of the problem will probably be eliminated by moving the ADC circuitry onto the control board. The success of the preamplifier and sampling circuitry is very encouraging as it indicates that the most fundamental and difficult part of the circuit is sound and can be applied in further development work.

5.0 X-RAY TESTING

The objectives of the x ray testing were to evaluate the spatial resolution of the SFRD and to perform and reconstruct a pseudoscan of a symmetrical object. The spatial resolution was evaluated by imaging a very fine slit aperture on the detector. Unfortunately, we were not able to perform the pseudoscan because of funding constraints.

In the proposal, we had planned to perform the experiments using a microfocal source at TFI Corporation in Connecticut. During the performance period of this project, a 420 kV x-ray source was activated at the ARACOR facility. By assembling appropriate collimation on this source and reducing the anode potential to 200 kV, we were able to carry out the project in-house.

5.1 The Experiment

The experiment consisted of placing slit collimation at the source and detector in order to image a fine x-ray pencil beam with the SFRD. The uncollimated x-ray source had an anode pattern consisting of two horizontal lines 5-mm long, separated by about 3 mm. Each of the lines is about 1.5 mm

thick (vertical height). In front of the source was placed a thick (4 in.) lead collimator with a horizontal slit (1mm x 5mm) through the center. The source slit consisted of a pair of closely spaced (100 microns) vertical Tungsten rods (16 mm diameter). The effective source was thus 100-microns wide, 1 mm high and located 240 mm from the anode surface. The x-ray tube was operated at 200 kV and 10 ma.

The detector slit was another pair of highly polished tungsten rods (16 mm diameter) separated at the top and bottom by a 6-micron mylar film producing a slit width of a few microns. This slit was placed immediately in front of the cryostat (50 mm from the reticon) and 440 mm from the source slit. Vertical detector collimation consisted of a pair of 3-mm-thick lead sheets placed between the slit and the cryostat with a vertical separation of 2mm. The x-ray pattern on the detector was thus approximately trapezoidal with a base width of about 15 microns (FWHM about 10 microns) and 2mm high.

After a careful alignment of the collimators, we were able to place the x-ray image approximately centered on a single detector pixel. The resulting image is shown in Figure 6, after background subtraction and averaging the right and left halves to remove the remaining assymetry, due to the slight misplacement of the x rays with respect to the pixel.

The measured response, shown in Figure 6, gives the net signal in each pixel as normalized to the central element. This point-spread function has two distinct components -- a very sharp central peak and a broader base. In the figure, we have fit the base with an exponential to visually separate the two. The sharp peak is essentially contained in the central and adjacent pixels giving it a FWHM just under 50 microns. The broader wings have a FWHM of about 140 microns and half of the total area.

The response of the SFRD was previously modeled as shown in Figure 7.⁽¹⁾ As in Figure 6, each histogram element represents a single 25-micron pixel. The spread of the response into the pixels adjacent to the center is due to transport of photoelectrons within the scintillator. The low background in this

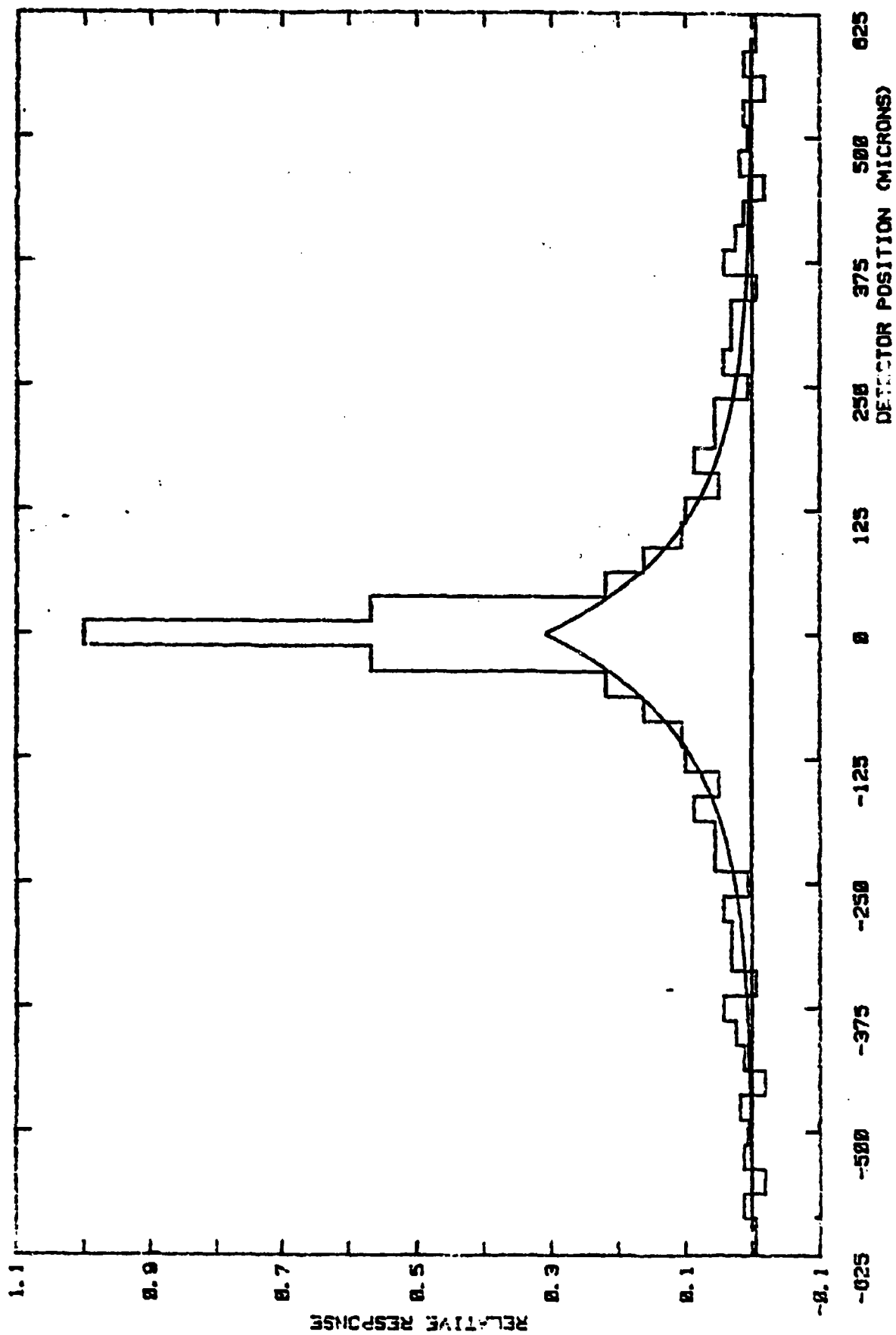


FIGURE 6. MEASURED RESPONSE OF SF60.

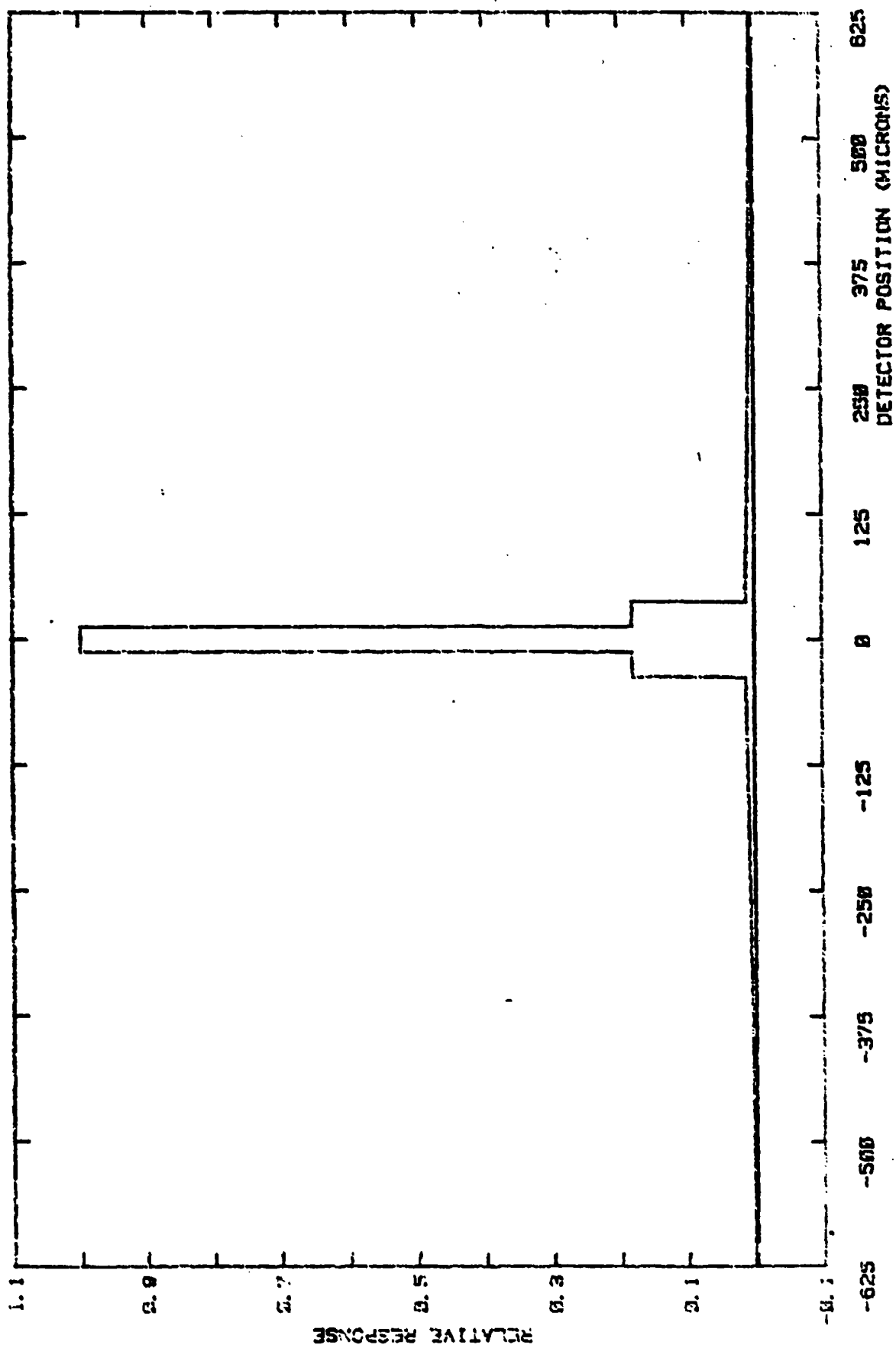


FIGURE 7. MODELLED RESPONSE OF SFRD.

figure is due to fluorescent x rays from the excited barium k-shell. This fluorescent component has a FWHM of 600 microns and 28% of the total response.

In comparing the modeled and measured response the similarity between the two central peaks is quite good. The correspondence would improve if we took into consideration the slight broadening in the measurement due to the finite width of the x-ray image.

On the other hand, the low wings shown in Figure 6 are too narrow and contain too much of the total area to be entirely attributed to the barium fluorescence. Our present interpretation is that the non-fluorescent portion is due to coherent scattering off of the tungsten detector slit. If so, this component will be greatly reduced in low-Z samples, because their x-ray attenuation is dominated by incoherent scattering which has a nearly isotropic distribution at these energies.

Our interpretation should be considered tentative at this time. Further experimental work will be required to confidently interpret the response. In addition, attention should be paid to the implications of x-ray scatter in the sample.

5.2 Assessment

At this point the spatial resolution of the SFRD is very promising. The sharp central response indicates that 25-micron sample resolution can be achieved with little or no deconvolution, provided our present interpretation of the low-level wings stands. If this base response is inherent in the SFRD, then it can be removed via deconvolution of the PSF from the data. The implication with respect to system performance would be that throughput would be reduced because of the improved sampling statistics required to overcome the deconvolution noise. We cannot quantify this factor at this time.

6.0 CONCLUSIONS

This project has contributed significantly to the development of the SFRD technology and to demonstrating its viability. At this point, we are confident that the required noise levels can be reached and that the detector response is adequate for the purpose. Clearly, work remains in eliminating the post-preamplifier noise and more experimental work is necessary to further understand the detector response and scattering effects in the sample.

The project undertook an ambitious slate of development issues. The cryostat, Reticon control circuitry and preamplifier stage performed up to their design goals, though noise pickup between the preamplifier and the data application system needs further reduction. The detector resolution was measured and showed resolving power appropriate to 25 micron image resolution. The only goal we were unable to address was the pseudoscan of a symmetrical ceramic object.

From the viewpoint of developing a high resolution Tomoscope, the technical risks associated with using a novel detector technology have been significantly reduced. The instrumental strategy of using the SFRD in a rotate-only geometry continues to appear promising.

REFERENCES

- (1) Smith, J. A., et. al., "An Improved NDE Capability for Aerospace Components," Final Report DNA Contract DNA001-84-C-0046, December 1984.
- (2) Simpson, R. W., "Noise in Large Aperture Self-Scanned Diode Arrays," Review of Scientific Instruments, 50, June 1979.